Structural Order and Orientation of Organometallic Pillars on Synthetic Fluorhectorite and Montmorillonite Surfaces

Faina Tsvetkov and John White*

Research School of Chemistry, Australian National University, G.P.O. Box 4, 2601, Australia

Received August 15, 1988

Pillared clays with controlled interpillar distances have been prepared by systematically varying the pillar and clay charges in metal–sarcophagine cage complex/clay systems. In some cases there is very high crystallinity—14 orders of *c*-axis diffraction having been observed. Adsorption isotherms have been determined that show that two separate shape-selective effects occur in these materials: (a) "molecular sieving" due to the interpillar gaps; (b) enhanced adsorption of hydrogen due to the pillar shape allowing penetration under the pillar. These effects are discussed by using molecular modeling calculations to simulate the porosity and available adsorbing surface.

Introduction

Smectites have a sandwich structure where negatively charged alumosilicate layers are separated by positively charged cations. The charge in fluorhectorite and montmorillonite arises from isomorphous substitution mainly in the middle of the clay layers (9.6-Å thickness).[1] When large inorganic and organic cations separate the clay sheets, sufficient interlamellar space is created[2-4] to allow a variety of adsorption and catalytic uses. These include chromatographic supports,[5] adsorbent,[6] and shape-selective and cracking catalysis.[7] For such applications control of the free lateral surface and pore size are important factors. This paper addresses this question for a model system.

In a previous paper[8] we proposed that pillaring of montmorillonites and fluorhectorite clays is governed essentially by charge balance and that when the charge distribution allows a structure to form whose two-dimensional lattice parameters correspond to the parameters of the supporting clay, the pillar structures are most stable. From this understanding of the pillaring process one can select pillaring agents and suitable clays to form the rigid structures needed for molecular sieving, catalyst, or slow-release formulations. Direct observation of interpillar distances were made recently[8] by X-ray powder diffraction from such well-oriented clays. The present paper correlates gas adsorption capacity with diffraction measurements of the pillar packing by using molecular graphics modeling programs to analyze the surfaces available to adsorption for different adsorbates. Mercury diamsar was chosen as the principal pillaring agent to optimize the in-plane X-ray diffraction (diamsar = 1,8-diamino-3,6,10,13,16,19-hexaazabicyclo[6.6.6]eicosane).

Experimental Section

Preparation of Pillared Smectite. Two smectites were used for pillaring: synthetic fluorhectorite (supplied by Prof. T. J. Pinnavaia, Michigan State University), $Li_{1.4}[F_4Si_8(Li_{1.4}Mg_{4.6})O_{20}]$, and sodium montmorillonite prepared by the procedure of Callaghan et al.[9] from natural montmorillonite (Osage, Wyoming bentonite, Wards Natural Science Establishment Inc., Rochester, NY). While fluorhectorite is a trioctahedral smectite, montmorillonite is dioctahedral, where the middle octahedral positions are filled with Al^{3+} and charge arises mainly from isomorphous substitution of Al^{3+} by Mg^{2+}. The general formula is $M^+_x[(OH)_4Si_8(Al_{3-x}Mg_x)O_{20}]$.[1] Pillaring agents were metal-sar and -diamsar cations.[10] Metal ions Co^{3+} and Hg^{2+} were used with sarcophagine cage $C_{14}N_6H_{32}$ (sar) and diamsar, a sarcophagine cage that has additional terminal amino groups $C_{14}N_6H_{30}(NH_2)_2$ (Figure 1).

A 0.2% suspension of smectite was dripped slowly into a solution of pillaring agent with vigorous stirring. The stirring was continued for 2 more hours. Then the suspension was centrifuged, and the pillared clay washed four times with water and air-dried on glass slide. The amount of cage molecule in solution usually exceeded by a factor of 4 the amount of the molecules that could be adsorbed on the surface under the chosen pH conditions. The preparation of Hg-diamsar clays is fully described in our previous paper.[8] (Co-diamsar)–fluorhectorite and (Co-sar)–fluorhectorite were prepared by the same procedure with a high excess of pillaring agent at pH values during the preparation of 5.6 and 4.2, respectively. Water content was determined for the air-dried clays by vacuum desorption on the microbalance followed by reweighing after equilibrium with atmospheric moisture (see below).

Instruments. All samples were analyzed after slow drying in air at room temperature and thus contain adsorbed water. The pillar concentrations were determined from the air-dried samples and corrected to pillar concentration per gram of dry clay by using the amount of adsorbed water for each sample as determined above. For fluorhectorite samples, 87% purity of initial clay was assumed,[8] and for 90% montmorillonite. Metals were determined by flame atomic absorption spectroscopy of solutions obtained by dissolving the sample in concentrated nitric acid. The automatic analyzer used was a Carlo Erba 1106. Sample combustion was followed by gas chromatographic separation of the resultant gases with a thermal conductivity detector for the C, H, and N determinations.

A Siemens D501-K710 X-ray powder diffractometer with a Cu target was used with sample in both reflection (scattering vector perpendicular to the layer plane) and in transmission mode to favor observation of *c*-axis and in-plane diffraction, respectively,

(1) Grim, R. E. *Clay Mineralogy*; McGraw-Hill Book Co.: New York, 1968; pp 77–92.
(2) Pinnavaia, T. J. Intercalated clay catalyst. *Science* **1983**, *220*, 365–371.
(3) Barrer, R. M. Expanded clay minerals: a major class of molecular sieves. *J. Inclusion Phenom.* **1986**, *4*, 109–119.
(4) Lahav, N.; Shani, U.; Shabtai, J. Cross-linked smectities. I Synthesis and properties of hydroxy-aluminum-montmorillonite. *Clays Clay Miner.* **1978**, *26*, 107–115.
(5) Mingelgrin, U.; Tsvetkov, F. Adsorption of dimethylanilines on montmorillonite in high-pressure liquid chromatography. *Clays Clay Miner.* **1985**, *33*, 285–294, and references within.
(6) Odom, I. E. Smectite clay minerals: properties and uses. *Philos. Trans. R. Soc. London, A* **1984**, *311*, 391–409.
(7) Adams, J. M.; Martin, K.; McCabe R. W. Clays as selective catalysts in Organic Synthesis. *J. Inclusion Phenom.* **1987**, *5*, 663–674.
(8) Tsvetkov, F.; White, J. Aggregation of organometallic complex pillars in synthetic fluorhectorite and montmorillonite. *J. Am. Chem. Soc.* **1988**, *110*, 3183–3187.
(9) Callaghan, I. C.; Ottewill, R. H. Interparticle forces in montmorillonite gels. *Faraday Discuss. Chem. Soc.* **1974**, *57*, 110–118.
(10) Comba, P.; Sargeson A. M.; Engelhardt, L. M.; Harrowfield, J. M.; White, A. H.; Horn, E.; Show, M. R. Analysis of trigonal-prismatic and octahedral preferences in hexaamine cage complexes. *Inorg. Chem.* **1985**, *24*, 2325–2327.

0897-4756/89/2801-0149$01.50/0

Table I. c Spacing and Limiting Water Capacity for Pillared Smectites at Room Temperature

clay	p, mM/g of clay mineral	c spacing, Å	water: limiting sorption S_m capacity, mM/g of clay mineral	water: m^2/g of clay mineral[b]
(Hg-diamsar)–montmorillonite I	0.255	16.74	8.39	631
(Hg-diamsar)–montmorillonite II	0.339	16.74	8.86	667
(Co-sar)–fluorhectorite	0.589	17.17	8.51	640 (529[a])
(Hg-diamsar)–fluorhectorite I	0.491	16.72	9.19	692
(Hg-diamsar)–fluorhectorite II	0.499	16.77	7.73	581
70 °C heated		15.2–15.6	4.64	349
(Co-diamsar)–fluorhectorite	0.540	16.84	7.36	554
(Hg-diamsar)–fluorhectorite III	0.640	16.79	7.80	587

[a] Reduced also by a factor of $S_p^{sar}/S_p^{diamsar} = 170/140 = 1.21$. [b] Assuming 12.5 Å^2 as the area occupied by a water molecule.

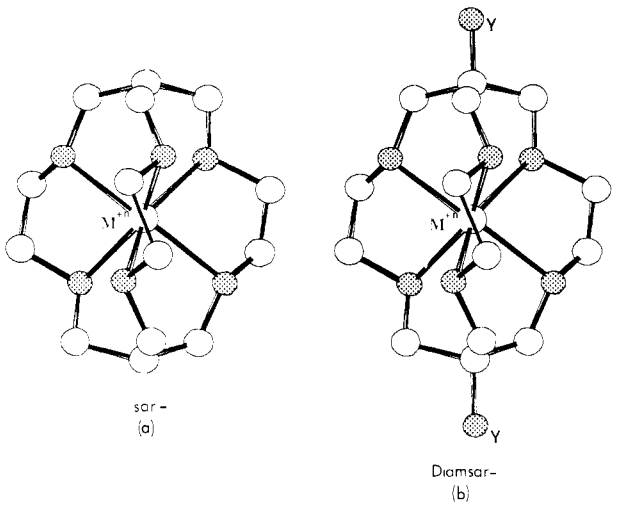

Figure 1. Structure of metal–sacorphagine cage pillars, where M^{n+} is Co^{3+} and Hg^{2+} and Y is NH_3^+ and NH_2: (a) sarcophagine; (b) diamsar–sarcophagine. Shaded circules represent amino groups, and empty circles represent carbon atoms; hydrogen atoms are omitted.

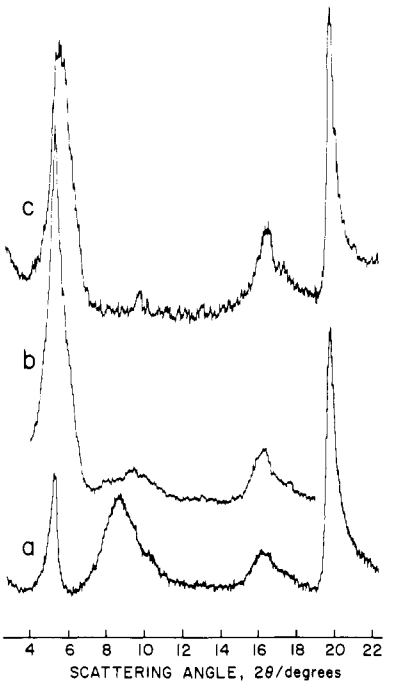

Figure 2. X-ray powder diffraction patterns in transmission mode of oriented samples of (a) oriented (Hg-diamsar)–fluorhectorite II, (b) (Hg-diamsar)–fluorhectorite II, heated at 70 °C, redispersed, and oriented by air drying, (c) oriented (Hg-diamsar)–fluorhectorite II, heated at 70 °C, and then sealed to prevent water uptake.

from the well-oriented samples. Samples for transmission were thin films of the clays produced by slow water evaporation, freely mounted in the X-ray beam. Determinations of the c-axis spacing were made from ground powder samples to avoid preferred orientation effects in comparisons with calculated intensities.

A Sartorious microbalance was used to measure adsorption isotherms for hydrogen and nitrogen at 77 K. Samples were pumped to constant mass, at room temperature and about 10^{-5} Torr, before commencing the gas adsorption. The amount of adsorbed and desorbed water was determined as follows: after pumping at 10^{-5} Torr (300 K) the samples were allowed to equilibrate with the atmosphere to constant mass for at least 24 h. The difference in weight after equilibration with air and in vacuum was taken as an amount of water adsorbed. The samples were again dehydrated at 300 K and 10^{-5} Torr before gas sorption. At least four measurements of water uptake were made for each clay.

Pillar Stability at the Clay Surface. As part of the synthetic chemistry a number of measurements were made to characterize the stability of clays pillared with mercury-diamsar. This pillar turned out to be unstable above 300 K and illustrates a worst-case condition for the sarcophagine cage pillars though its desirability for X-ray diffraction offsets this.

Dialysis. Four clays, (Hg-diamsar)–fluorhectorite III, (Hg-diamsar)–fluorhectorite I, (Hg-diamsar)–montmorillonite II, and (Hg-diamsar)–montmorillonite I were dialyzed, and the concentration of pillar remaining in the clay was determined from microanalysis of N, C, and Hg. The pillar concentration does not change significantly in all samples except (Hg-diamsar)–fluorhectorite III, where dialysis leads to a decrease in pillar concentration in the clay at about 10%. Only this clay was prepared in basic conditions (pH 8) from a solution containing pillaring agent in deprotonated form. The charge of the pillars in (Hg-diamsar)–fluorhectorite III is lower than, for example, in (Hg-diamsar)–fluorhectorite I, which was prepared at pH 3.5. We suppose that upon dialysis in water, the pillars from (Hg-diamsar)–fluorhectorite III increase their charge due to protonation of the side amino groups and that this causes the release of excess pillars from the surface. The pH value of the suspension during the preparation influences the charge of the pillars both in solution and on the surface. In its turn the pillar charge on the surface determines the pillar concentration in the clay.

X-ray Powder Diffraction. We have found that heating at 70 °C or even pumping for several days at room temperature may partially decompose mercury-containing pillar ions, leading to a decrease of clay c spacing from 16.8 to 15.6–15.2 Å.

The change in clay color from white to yellowish, the reduced amount of mercury extractable from the clay in analysis, and the presence of a peak at 200 (Hg) in the mass spectra all suggest that the process has several stages. A possible scheme is that at first, Hg^{2+} leaves the cage to react with surface water (eq 1) and then

$$Hg^{2+} + H_2O = HgO + 2H^+ \quad (1)$$

$$HgO = Hg + \tfrac{1}{2}O_2 \quad (2)$$

mercury oxide is partially decomposed to mercury and oxygen (eq 2). The c spacings of heated samples are listed in Table I.

Figure 2 shows the X-ray powder diffraction pattern for oriented samples in transmission mode for (a) nonheated (Hg-diamsar)–fluorhectorite II, (b) heated at 70 °C and redispersed in

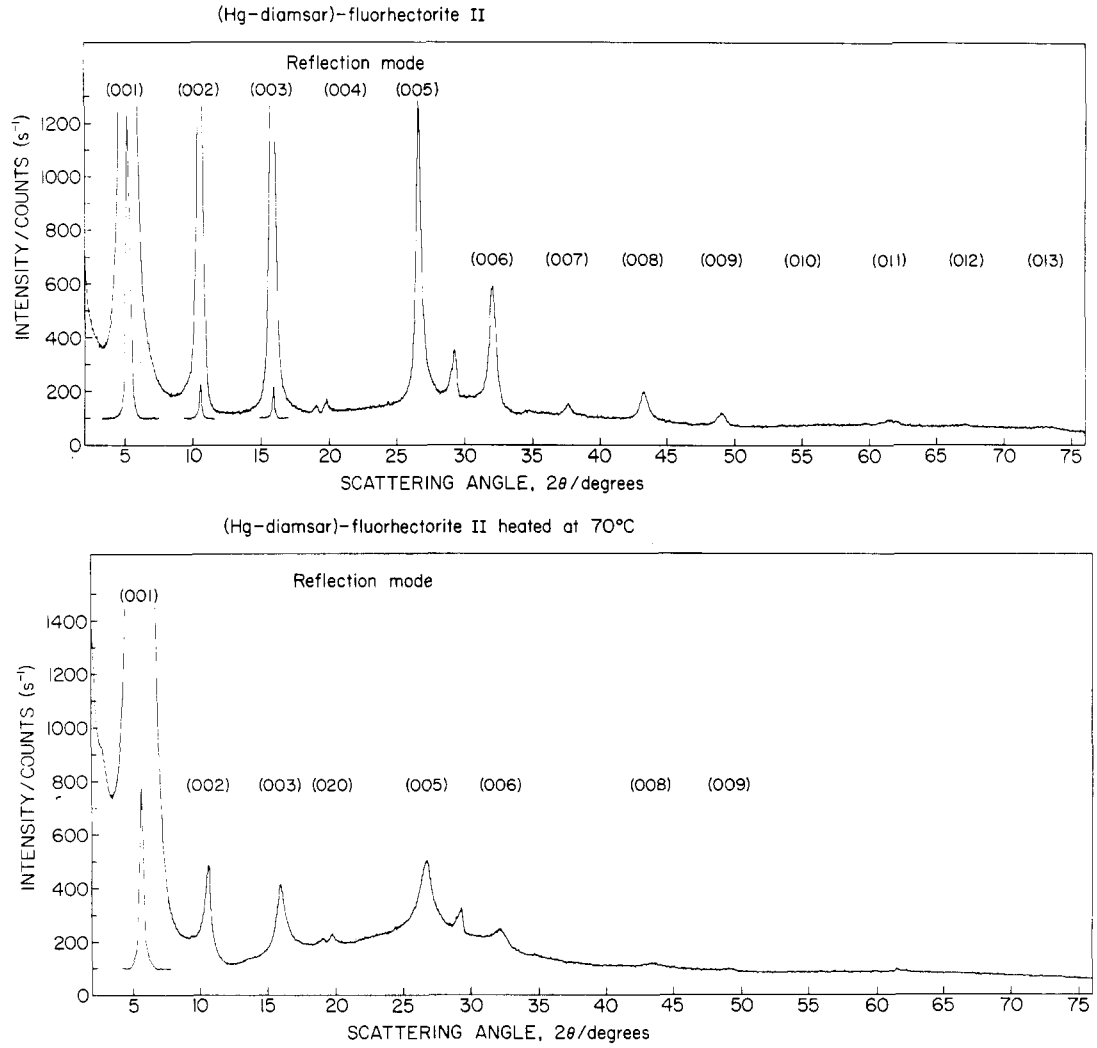

Figure 3. X-ray powder diffraction patterns from oriented samples in reflection mode of (top) (Hg-diamsar)–fluorhectorite II (the intensities of (001), (002), (003) peaks are 20 times decreased) and (bottom) from a redispersed and dried (Hg-diamsar)–fluorhectorite II after heating at 70 °C (the intensity of small (001) peak is 20 times decreased); Cu Kα radiation.

water during sample preparation, and (c) heated at 70 °C after the preparation of the oriented sample and sealed before running spectra to prevent contact with the air to avoid water adsorption. Figure 3 (top) shows the X-ray powder diffraction pattern in reflection mode for unheated (Hg-diamsar)–fluorhectorite II and for the same sample heated at 70 °C and then redispersed in water and then air-dried (Figure 3, bottom). The intensity ratio I_{001}/I_{020} in transmission mode gives a qualitative indication of the quality of packing in these samples. This ratio is equal to 0.37 for nonheated (Hg-diamsar)–fluorhectorite II but rises to 1.15 for the heated sample, showing lower anisotropy in the clay sheets diffraction on heating. The *c* spacing for the redispersed sample is close to the *c* spacing for nonheated (Hg-diamsar)–fluorhectorite II and equal to 16.45 Å, while the *c* spacing for heated and sealed samples is 15.2–15.6 Å. There is some indication here of the need for water to be associated with the pillar to achieve maximal *c* spacing.

Only the X-ray powder diffraction pattern, in transmission mode, for nonheated (Hg-diamsar)–fluorhectorite II (Figure 2a) shows the well-resolved signal corresponding to in-plane interpillar distances. Redispersed (Hg-diamsar)–fluorhectorite II shows a broad signal that may be assigned as a superposition of several peaks. One peak at 10.8 Å corresponds to the unheated in-plane distribution, and two new signals (at 9.2 and 8.8 Å) correspond to smaller interpillar distances. Thus during redispersion, pillars with smaller charge form new structures on the clay surface. In the heated and then sealed sample, no rearrangement due to subsequent water sorption was possible, and decomposition or disordering of the pillars leads to almost complete absence of pillar–pillar diffraction near $d \sim 9.2$ Å.

Results

Diffraction and Pillar Orientation with Respect to the *c* Axis. The diffraction pattern of well-oriented (Hg-diamsar)–fluorhectorite II for which 14 orders of the *c*-axis diffraction are resolved is shown in Figure 3, top. The effective real space resolution is about 2 Å, sufficient to qualitatively test models for the orientation of the pillar relative to the *c* axis. Structure factors and relative intensities for a powder specimen were calculated for constant pillar packing density and four models of orientation of the ellipsoidal pillar relative to the *c* axis. The appropriate Lorentz and absorption corrections were made. As there are 22 nitrogen and carbon atoms for each heavy atom in the pillar, light- and heavy-atom contributions to the molecular scattering length are about equal at low angles. In models A and B the N–N axis of the pillar was oriented perpendicular to the *c* axis (Figure 4a,b); in model C the N–N axis of the pillar was parallel to the *c* axis (Figure 4c). For the fourth model (D) the angle of N–N axis of the pillar the with *c* axis was 45°.

The calculated/observed relative intensities agree best for the models A and B, where the N–N axis is parallel to the clay surface. The least-squares refinement factor is equal to 11.5, 9.4, 45.8, and 32.8 for models A, B, C, and D, respectively. No choice between models A and B can be made. Only this orientation will be used in the Chem-X[11] modeling discussed below. The parallel orientation

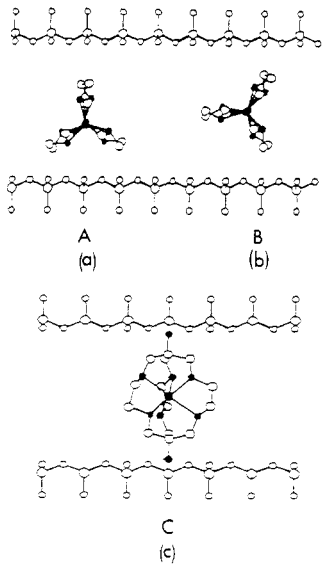

Figure 4. Different orientations of the pillar molecule on a fluorhectorite surface viewed along the clay surface: A and B, N–N axis of the pillar parallel to the clay surface; C, N–N axis of the pillar perpendicular to the surface.

also gives the closest c axis to that which is observed.

All Hg-diamsar clays showed almost the same c spacing (Table I). There was a slight trend in fluorhectorites for the c spacings to grow with the increased pillar in plane density. For example, with pillar concentrations of 0.35 and 0.43 mM/g of compound in (Hg-diamsar)–fluorhectorite I and (Hg-diamsar)–fluorhectorite III, respectively, the clay c spacing changes from 16.72 to 16.79 Å. the c spacing in Co^{3+}-containing fluorhectorites is somewhat higher (up to 16.8 Å for (Co-diamsar)–fluorhectorite and 17.17 Å for (Co-sar)–fluorhectorite). The difference in c spacings of Co-diamsar and Co-sar pillared clays suggests that the NH_3^+ of diamsar enhances the overall electrostatic attraction of the pillar to the negatively charged clay surface and is consistent with a pillar orientation with the N–N axis parallel to the clay surface.

Adsorption of Water. Because the diamsar pillared clays were sensitive to heating above 300 K, all gas adsorption measurements were made on material dehydrated by extensive pumping to 10^{-5} Torr at room temperature. Such dehydrated clays take up a lot of water when exposed to the atmosphere, and this is method was used to estimate limiting water adsorption capacity at 300 K.

Effect of Pillar Concentration on Water Adsorption. Using 12.5 $Å^2$ as the area occupied by the water molecule, we may convert the limiting water uptake (in moles) into the surface occupied by the water assuming monolayer coverage. This surface per gram of clay mineral is shown as function of pillar concentration in the clay galleries, in Figure 5. (That is, a correction has been made to the weight of the adsorbent to take away the mass of the pillars.) The dotted line is the best least-squares fit to all points, and the solid line is least-squares fitted with fixed intercept equal to the calculated specific surface area, A_{tot} (750 m^2/g of clay mineral) of the clays used.

If we define the clay surface area taken up by each pillar as S_p and the pillar concentration in moles per gram of starting clay, p, then the clay surface area available for water adsorption, S_w, is given by

$$S_W = A_{tot} - N_0 S_p p \quad (3)$$

(11) CHEM-X, Chemical Design Ltd, Oxford, 1986, reference manual.

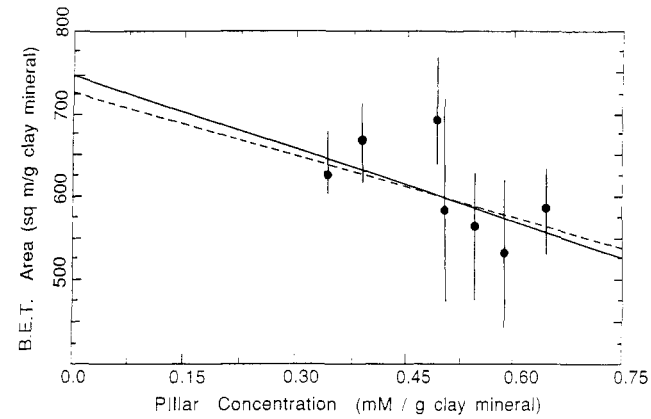

Figure 5. Dependence of the pillared clay surface area (m^2/g of clay mineral), determined by water adsorption, on pillar concentration (mmol/g of dry clay mineral). Pillar concentration was calculated as average for N, C analysis in air-dried samples, and water content was calculated from the microbalance experiment. The dotted line is a least-squares fit to all points; the solid line is a least-squares fit with fixed intercept (A_{tot} = 750 m^2/g).

where N_0 is Avogadro's number. The dotted line fitting this expression to the data of Figure 5 gives A_{tot} = 727 m^2/g of clay mineral and S_p = 43.2 $Å^2$ (and S_p = 50 $Å^2$ for the solid line). The water adsorption data are summarized in Table I.

There appears to be little hindrance to water penetration into the structure, and hydrogen-bond formation with surface oxygen[12] as well as hydration of the pillar edge amino groups may help this. As the maximal cross-sectional area of a diamsar pillar is about 170 $Å^2$, it is obvious that some water must be tightly bound by pillars or that the maximum cross section of the pillar is not an appropriate quantity for comparing to experimental values of S_p. We come back to modeling of the clay/water/pillar system in the Discussion.

The measured values of water adsorption in heated samples are highly scattered and vary from 2.2 mM/g of clay mineral to 6.3 mM/g. In heated (Hg-diamsar)–fluorhectorite II water molecules cover, on average, a much smaller area than in nonheated samples. The caly area occupied by one pillar molecule obtained from experiments on water adsorption was estimated equal to 42.3 $Å^2$ for nonheated (Hg-diamsar)–fluorhectorite II and 133 $Å^2$ for the heated material. This is consistent with an increased surface covered by, for example, the flattened pillar cage after Hg^{2+} has been driven out.

Adsorption Isotherms at 77 K for Nitrogen and Hydrogen. Adsorption isotherms at 77 K for nitrogen and hydrogen on different pillared clays have been determined by using the microbalance. We have systematically changed the clay and pillar charges to alter the lateral packing and hence the adsorption potentials at the adsorption site. All isotherms we measured by admitting a dose of gas, measuring the pressure above the sample after temperature equilibration, and measuring the sample mass as a function of time to constant mass.

Figure 6 shows the isotherms for nitrogen and hydrogen adsorption for each clay sample. On each isotherm the arrows indicate the determinations of water uptake also. The differences between Figures 6d and 5e show the strong reduction in surface areas produced by heating at 70 °C. The effects of increased in-plane pillar packing density in (Hg-diamsar)–fluorhectorite III (Figure 6f) are also clear—especially from the form of the hydrogen isotherm, which indicates saturation of microcapillary adsorption sites at low pressures.

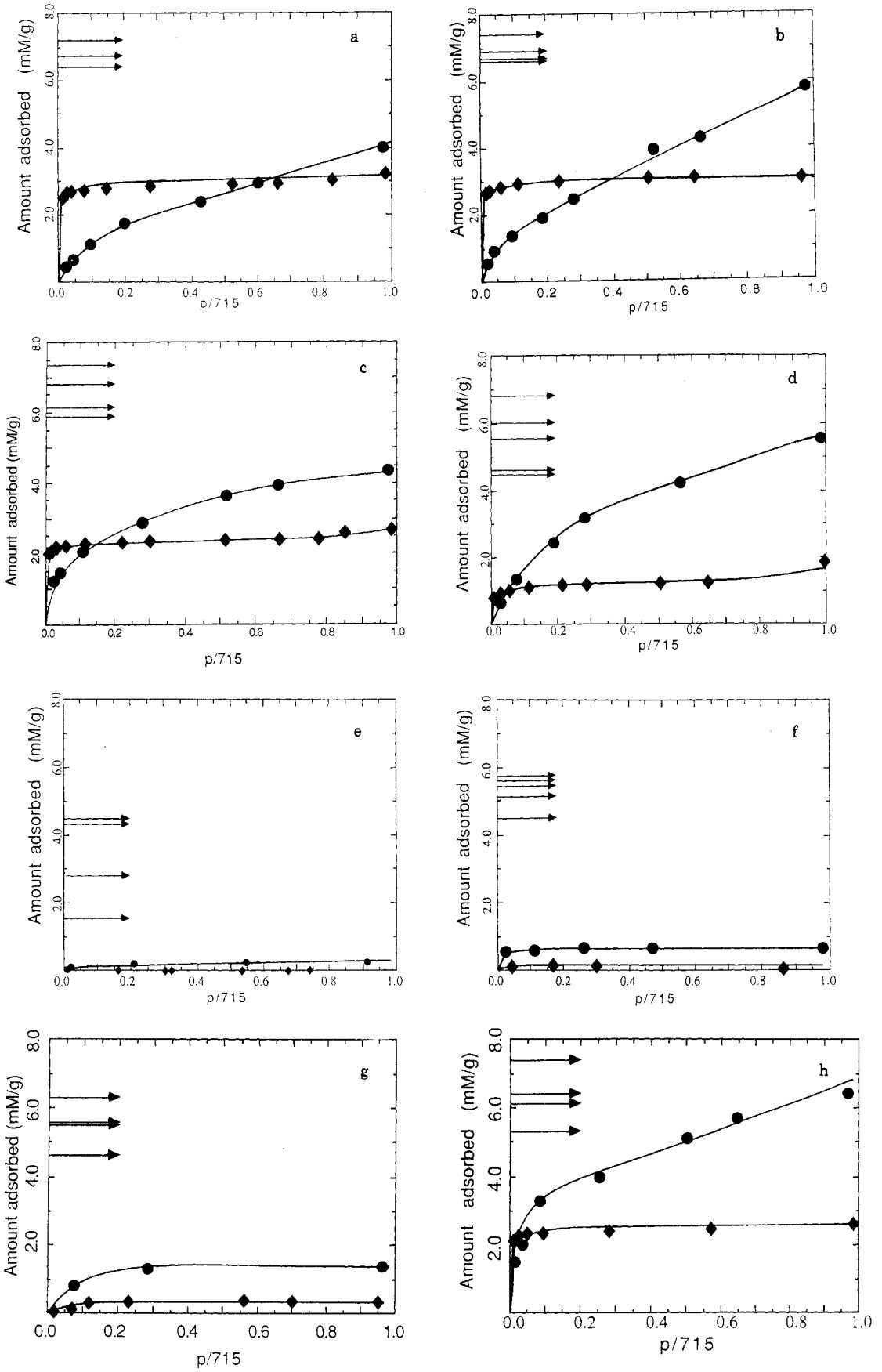

Figure 6. Adsorption of water (arrows), nitrogen (diamonds), and hydrogen (circles) on (a) (Hg-diamsar)–montmorillonite I, (b) (Hg-diamsar)–montmorillonite II, (c) (Hg-diamsar)–fluorhectorite I, (d) (Hg-diamsar)–fluorhectorite II, (e) (Hg-diamsar)–fluorhectorite II heated, (f) (Hg-diamsar)–fluorhectorite III, (g) (Co-diamsar)–fluorhectorite, and (h) (Co-sar)–fluorhectorite. The amount of adsorbate is expressed in mM of adsorbate/g of dry compound.

Table II. Dependence of Adsorption of Hydrogen and Nitrogen Molecules in Pillared Smectites upon Their Structure

clay	pillar numeral charge	pillar concn, mM/g of clay mineral	charge from pillar concn[a]	interpillar spacing (X-ray), Å	limiting sorption capacity hydrogen–nitrogen k[b] at 700 mmHg, mM/g of clay mineral			BET area hydrogen[c]–nitrogen[d] K,[e] m²/g of clay mineral		
(Hg-diamsar)–montmorillonite I	+4	0.255	+3.9	15.03	4.47	3.93	1.14	318	358	0.89
(Hg-diamsar)–montmorillonite II	+2	0.339	+2.9	12.7	6.54	4.13	1.58	397	402	0.99
(Co-sar)–fluorhectorite	+3	0.589	+3.0		8.38	3.58	2.34	524	331	1.58
(Hg-diamsar)–fluorhectorite I	+4	0.491	+3.7	10.8	6.23	3.59	1.74	480	330	1.45
(Hg-diamsar)–fluorhectorite II	+3	0.499	+3.6	10.77	7.41	2.23	3.32	675	167	4.04
(Co-diamsar)–fluorhectorite	+3	0.54	+3.3	(10.02)	1.75	0.33	5.30	145[f]	48[c]	3.02
(Hg-diamsar)–fluorhectorite III	+2	0.64	+2.8	9.48	0.96	0.24	4.00	78	24	3.25

[a] CEC for montmorillonite = 1.0 mequiv/g, and CEC for fluorhectorite = 1.8 mequiv/g.[8] [b] k is equal to ratio of maximal sorption capacity of hydrogen and nitrogen. [c] Surface area was calculated BET equation, where fitting was made in the pressure range from 65 to 400 mmHg. [d] Surface area was calculated from BET equation, where fitting was made in the pressure range from 0 to 500 mmHg. [e] K is equal to ratio of hydrogen and nitrogen BET surface areas. [f] Whole range, average from two measurements.

Gas Adsorption as a Function of Pillar Concentration on the Surface. (a) Nitrogen Adsorption Isotherms: Montmorillonites. With the relatively low layer charge in these clays the pillar packing in montmorillonites is more sparse than for the fluorhectorites. The surface area of a given pillared clay sample, in m²/g of clay mineral units, was determined by the BET method.[13] M, equal to the amount (in moles) of vapor adsorbed at monolayer coverage per unit weight of the pillared clay, was calculated from the Langmuir isotherm:

$$P/m = P_0/bM + P/M \quad (4)$$

where P is a vapor pressure at which m moles of vapor per unit weight of the adsorbent is adsorbed, and P_0 is equal to 715 mmHg. M is equal to a (slope)$^{-1}$ of the experimental plot of P/m versus P. All of the nitrogen adsorption isotherms corresponded well with Langmuir isotherms for monolayer coverage, and Table II summarizes the results.

(b) Nitrogen Adsorption Isotherms: Fluorhectorites. In (metal-diamsar)–fluorhectorites the high surface charge and consequently denser pillar packing causes the nitrogen adsorption to decrease very rapidly with increased pillar concentration. The specific surface is almost twice as big in (Hg-diamsar)–fluorhectorite I compared with (Hg-diamsar)–fluorhectorite II and is very small in (Co-diamsar)–fluorhectorite and (Hg-diamsar)–fluorhectorite III (measured free surface areas are 48 and 24 m²/g, respectively). This drop in adsorption is not associated with a decrease in c spacing as in the case of heated (Hg-diamsar)–fluorhectorite II but rather is caused by the decrease of the interpillar distances. We believe it is a molecular sieving effect. For both (Hg-diamsar)–fluorhectorite III and (Co-diamsar)–fluorhectorite the center-to-center interpillar distances are too small (10 and 9.48 Å, respectively) for nitrogen to pass into the pillared structure. By contrast in (Hg-diamsar)–fluorhectorite I all of the clay surface not occupied by pillars is available for nitrogen adsorption. The data are summarized in Table II.

(c) Hydrogen Adsorption: Montmorillonites and Fluorhectorites. In (Hg-diamsar)–montmorillonite I and (Hg-diamsar)–montmorillonite II interpillar free distances for all possible relative orientations are larger than 4 Å. The nitrogen molecules and a fortiori, hydrogen, may pass easily into the structure. A model of (Hg-diamsar)–montmorillonite II (Figure 7, top) confirms this.

To be more quantitative an estimate of the BET areas for hydrogen was made by using eq 4 mainly in the pressure range 65–400 mmHg. The intercept of this plot is without meaning, but the isotherm fits the data well, giving not unreasonable M values.

The free surface areas of pillared montmorillonites measured by adsorption of hydrogen are bigger than those measured by adsorption of nitrogen (taking standard cross-sectional areas per molecule of 12.3 and 16.2 Å² for H_2 and N_2, respectively[14]). For (Hg-diamsar)–montmorillonite I and II this difference is not significant, but for all other clays it is well marked. The ratio of clay surface occupied by hydrogen to the clay surface occupied by nitrogen ($K = S_{hyd}/S_{nit}$) changes from 1.45 in (Hg-diamsar)–fluorhectorite I to 3.25 in (Hg-diamsar)–fluorhectorite III. Although nitrogen penetration into the structure could have been reduced somewhat due to smaller free interpillar distances, the data indicate an effectively larger free clay surface available for the smaller hydrogen molecules.

The limiting sorption capacity at 77 K is very high for (Co-sar)–fluorhectorite (8.38 mM/g), and relative adsorption capacity for hydrogen and nitrogen (k) is also high (2.34), especially so for (Co-diamsar)–fluorhectorite (k = 5.3). In mercury-containing fluorhectorites k increased from 1.74 in (Hg-diamsar)–fluorhectorite I to 4.0 in (Hg-diamsar)–fluorhectorite III.

Discussion

The extent to which the simple geometrical model of eq 3 is valid for nitrogen adsorption by all of the samples is shown by Figure 8, top. Here the BET surface area is plotted as a function of pillar concentration (reduced to m²/g of clay mineral and mmol/g of clay mineral respectively to avoid confusion due to the changed density of the pillared clays as the pillar concentration increased). Least-squares fitting gives A_{tot} = 684 m²/g of clay mineral (in good agreement with the known clay unit cell and molecular weight A_{tot} = 750 m²/g of clay mineral) and a pillar area 166 Å². This latter figure is close to maximal cross-sectional area of a diamsar pillar lying with the N–N axis parallel to the clay surface (S_p^{calcd} = 170 Å², Tables III and IV). The spread of points is, however, larger than the experimental errors in determining the BET areas, and so we must presume some as yet uncontrolled variability in sample preparation.

Two possible factors are the extent of dehydration by pumping for different clays and the degree of pillar rota-

(12) Farmer, V. C. The characterization of adsorption bonds in clays by infrared spectroscopy. *Soil Sci.* **1977**, *112*, 62–68.
(13) Van Olphen, H. *Clay Colloid Chemistry*; Wiley: New York, 1977; p 87.
(14) McClellan, A. L.; Harnsberger, H. F. Cross-sectional areas of molecules adsorbed on solid surfaces. *J. Colloid Interface Sci.* **1967**, *23*, 577–599.

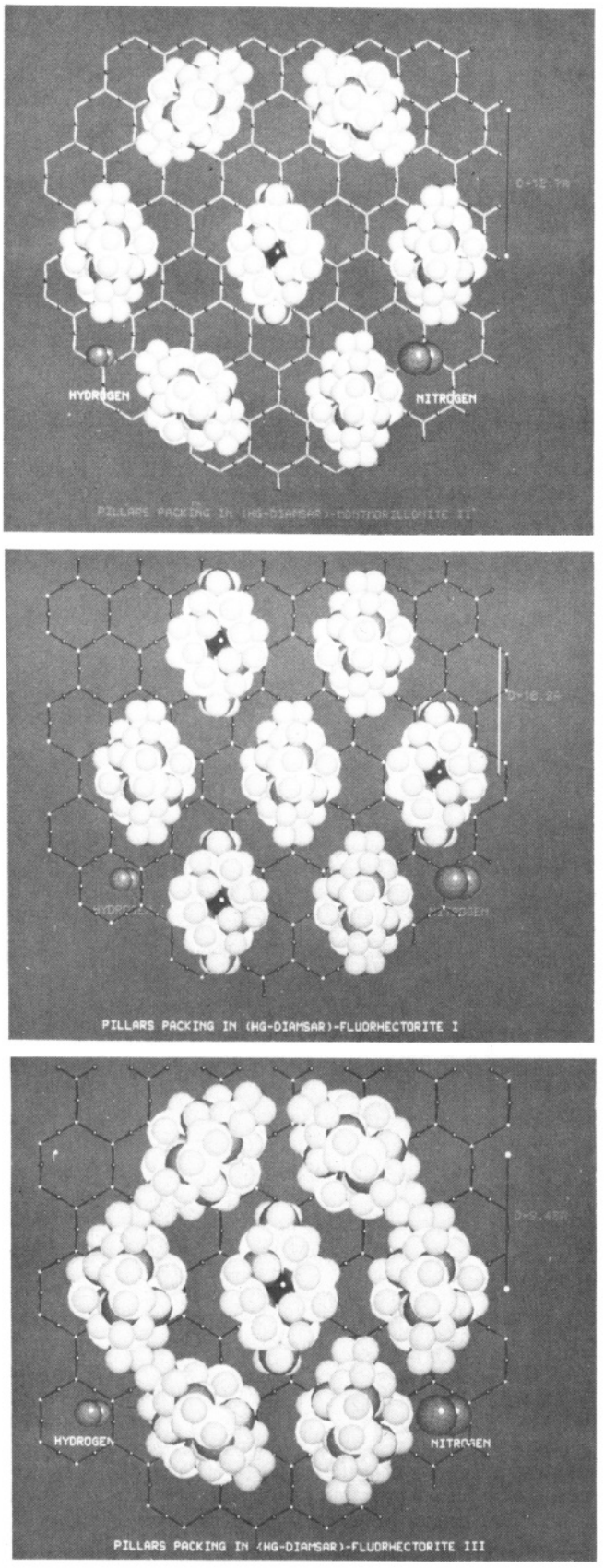

Figure 7. Model for hexagonal packing of pillars viewed perpendicular to the clay surface for (top) (Hg-diamsar)–montmorillonite II, (middle) (Hg-diamsar)–fluorhectorite I, (bottom) (Hg-diamsar)–fluorhectorite III. Seven pillar molecules are in the clay plane. D is the observed interpillar distance. H_2 and N_2 are hydrogen and nitrogen, respectively, with the H–H bond equal to 0.75 Å and the N–N bond equal to 1.1 Å. The photographs are made from the terminal screen.

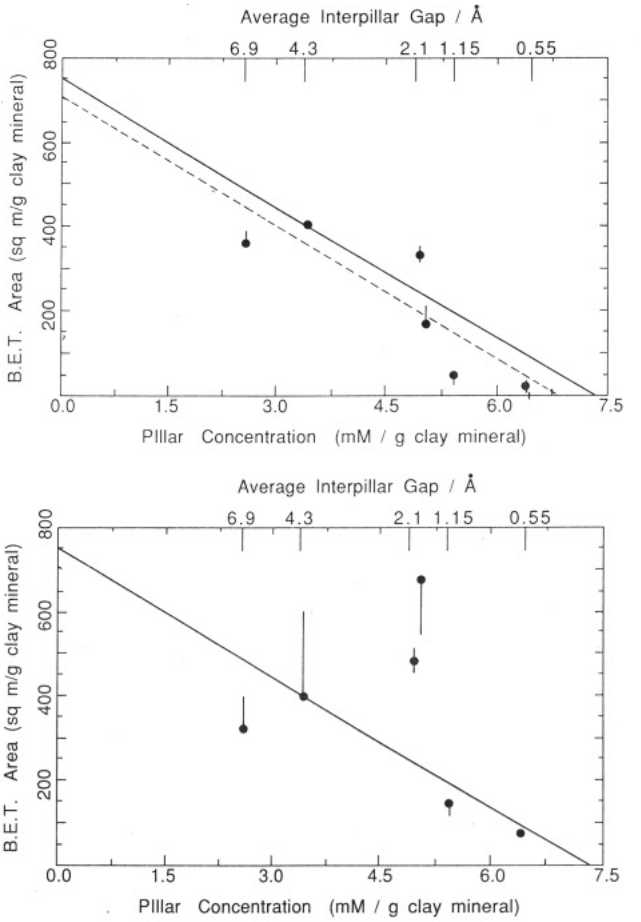

Figure 8. BET areas per gram of clay mineral for (top) nitrogen and (bottom) hydrogen as a function of pillar concentration in the clay. The solid line is a calculated dependence, where S_{clay} = 750 m^2/g of clay mineral and S_p = 170 $Å^2$; the dotted line is the least-squares fit to experimental data.

tional order in the pillar planes. For (Hg-diamsar)–montmorillonite I the lower than expected area is difficult to ascribe to these factors. At this point, pillar centers are 17.1 Å apart, and so there may be some bending of the clay sheets. Nevertheless, the nitrogen adsorption data are in qualitative agreement with the simple geometrical model based on a standard clay sheet surface area and approximately cylindrical pillars whose cross section is the maximum cross section of the diamsar molecule.

Effect of Pillar Orientation and Size. The nitrogen data, above, show the sieving effect for a given pillar of gradually increasing the pillar in-plane packing density. Taking the rotationally averaged diamsar pillar diameter presented to nitrogen as ca. 10.4 Å, we see that a critical pillar–pillar gap between ca. 4 and 2 Å cuts off access to large areas of the clay surface for nitrogen.

The large decrease in nitrogen adsorption for (Hg-diamsar)–fluorhectorite I compared with (Hg-diamsar)–fluorhectorite II can be understood by using molecular graphics. In this range of interpillar distances even a very slight decrease of interpillar distances assuming fixed pillar orientation could be sufficient to influence nitrogen penetration. This is illustrated in Figure 7, middle. Second, the gaps or free distances (distances between edges of pillars) become smaller for nonparallel orientation of pillars, and this is more likely in (Hg-diamsar)–fluorhectorite II than in (Hg-diamsar)–fluorhectorite I when one amino group is protonated and one is not protonated. In this compound also a nonparallel orientation of pillar molecules is energetically preferred and favored by the

Table III. Cross-Sectional Areas of the (Hg-diamsarH$_2$)$^{4+}$ Pillar at Different Distances from the Clay Surface[a]

z coord of the calcd pillar sect[b]	dist from the surface,[c] Å	contributional cross-sect area of the surface, Å		total cross-sectional area of the pillar, Å^2	
		model A	model B	model A	model B
4.63	1.3	12.4	20.9		
12.17		18.2	21.9	30.6	34.3
4.83	1.5	22.1			
11.97		20.0		42.1	
5.13	1.8	36.4	27.4		
11.67		25.1	27.3	61.5	54.7
5.33	2.0	46.6	31.3		
11.47		28.7	30.0	75.3	61.3
5.63	2.3	59.3	34.9		
11.17		31.8	34.1	91.2	69.0
6.13	2.8	72.9	46.4		
10.67		38.4	49.1	111.3	95.5
6.33	3.0	76.5	53.0		
10.47		39.8	57.8	115.4	110.8
6.83	3.5	82.4	68.1		
9.97		43.6	70.3	126.0	138.4
7.53	4.2	84.9[d]			
9.27		56.6		141.5	
8.15	5.3/4.8	81.5			
8.4			78.3[d]		156.6

[a] Nitrogen radius = 1.5 Å, hydrogen radius = 1.0 Å, carbon radius = 1.6 Å, surface oxygen z coordinate = 3.33 Å, and 16.8 − 3.33 = 13.47 Å, z coordinate of Hg_1 = 8.15 Å for model A and 8.4 Å for model B; pillar orientation is as shown in Figure 4a,b for model A and B, respectively. [b] z coordinate is taken in direction of c axis, c spacing is 16.8 Å, and a z coordinate of the center of the lower plate is equal to zero. [c] The distance is taken from the center of the clay surface oxygen. [d] A maximal cross-sectional area is equal to 170 Å^2 for model A and 157 Å^2 for model B.

R–H_2N:···$^+NH_3$–R, i.e., the nitrogen lone electron pair to positively charged amino group interaction, and so access to nitrogen molecules may be closed off. An alternative explanation is that for such narrow pores blocking by any pillar decomposition products becomes a much more important effect.

(Co-sar)–fluorhectorite (which has hydrogens instead of the terminal amino groups on the pillar, Figure 1) has a smaller pillar diameter than Co-diamsar, and so the free interpillar distances are increased. The difference can be as large as 5 Å, and there is easier nitrogen penetration into the pillared structure. The clay free surface area measured by nitrogen adsorption (Figure 6g,h) increases sharply from 48 m^2/g of clay mineral in (Co-diamsar)–fluorhectorite to 331 m^2/g in (Co-sar)–fluorhectorite, an effect due to increased free interpillar distances because of decreased pillar cross-sectional area. The corresponding surface area measured by hydrogen adsorption increases from 145 m^2/g to 524 m^2/g, and so hydrogen molecules in (Co-sar)–fluorhectorite occupy a major part of clay surface. There is no hindrance for hydrogen adsorption. S_{hyd}/S_{nit} ratio is 1.58 and 3.02 for (Co-sar)–fluorhectorite and (Co-diamsar)–fluorhectorite, respectively.

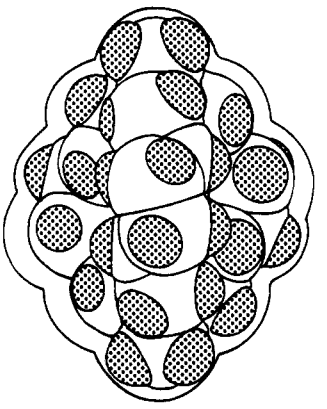

Figure 9. Model of (Hg-diamsarH$_2$)$^{4+}$ ion with its N–N axis parallel to the clay surface, viewed perpendicularly to the clay surface plane. Hydrogen atoms are shaded. An area inside the solid contour is the maximum cross-sectional area of the ion.

Pillar Shape Effects and Hydrogen Adsorption. The situation for hydrogen adsorption by mercury-diamsar pillared smectites is qualitatively different from that for nitrogen adsorption. This can be seen from Figure 8, bottom, where the line is as that in Figure 8, top, expected from the known clay surface area and maximal pillar areas. At close pillar spacings much more hydrogen than nitrogen can be adsorbed, an effect that is particularly marked for (Hg-diamsar)–montmorillonite II and (Hg-diamsar)–fluorhectorite I and II. The data, though subject somewhat to which range of the isotherm is fitted (shown by the range of error bars), appear even to show an increase in hydrogen-adsorption capacity as the pillars are packed more densely. We have used packing programs in the CHEM-X molecular graphics package to estimate the accessible areas of the various structures.

Molecular Graphics Models. The first thing is to define accurately the shape of the approximately ellipsoidal mercury-diamsar molecule so that microporous structures created by dense pillar packing can be modeled. Figure 9 shows the Hg-diamsar molecule as it would be oriented with the N–N axis parallel to the clay plane in model A or B below. An external van der Waals contour showing the maximum cross section is drawn, but it is obvious that contours at different heights from the clay plane would have much smaller cross sections. This can be seen also from the side elevations of Figure 10.

With CHEM-X, the cross-sectional area of the pillar at different heights from the clay surface was calculated. The crystal structure for (Hg-diamsarH$_2$)$(NO_3)_4^{3+}$,[10] the experimental c spacings of the pillared clay, and the smectite structure[15] were used to define the interatomic distances.

Table IV. Surface Occupied by Pillars (S_p, Å^2) Measured by Hydrogen, Nitrogen, and Water Adsorption in Pillared Smectites

	water		hydrogen			nitrogen	
	S_{av}[a]	S'_m[b]	S_p	S'_{BET}[b]	S_p	S'_{BET}[b]	S_p
(Hg-diamsar)–montmorillonite I	486	411	75	207	279	233	253
(Hg-diamsar)–montmorillonite II	366	327	29	194	172	197	167
(Co-sar)–fluorhectorite	211	180	31	148	63	93	118
(Hg-diamsar)–fluorhectorite I	252	234	18	162	90	111	141
(Hg-diamsar)–fluorhectorite II	249	194	55	225	24	56	193
(Co-diamsar)–fluorhectorite	230	170	60	45	185	15	215
(Hg-diamsar)–fluorhectorite III	194	152	42	20	174	6	188

[a] $S_{av} = A/(pM)$, where A is an area of a unit clay cell and is equal to 93 Å^2, M = 750 is its molecular weight. [b] $S'_m = S_m/(pN)$ and $S'_{BET} = S_{BET}/(pN)$.

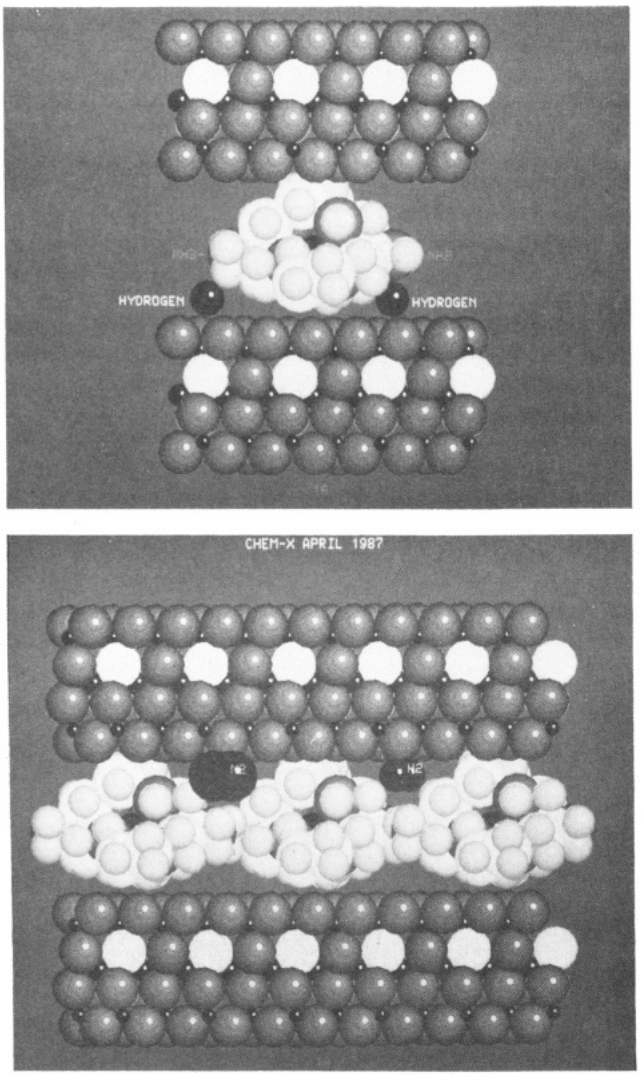

Figure 10. Model of (Hg-diamsarH)$^{3+}$ ion (on the left side NH_2 group and on the right side NH_3^+) between two clay layers in (Hg-diamsar)–fluorhectorite II. Interlayer distance corresponds to c spacing equal to 16.8 Å: (top) two hydrogen molecules shown on the level 2.3 Å from the surface; (bottom) model of the same clay with two amino groups protonated. Hexagonal packing of the pillars, interpillar distance of 10.77 Å; viewed along the clay surface. The photographs are made from the terminal screen.

The CHEM-X program calculates molecular volumes and molecular cross-sectional areas for chosen sections of the molecule whose size is defined by van der Waals radii. The cross-sectional areas were calculated only for models A and B, which give the closest fit to c-axis X-ray diffraction for this system.

To point out any effects due to penetration of adsorbed molecules under pillar "eaves", we take the known area of a clay surface A_{tot} m^2/g of clay mineral (from crystallography), the surface areas (m^2/g clay mineral) determined by for hydrogen and nitrogen adsorption, S, and define experimental effective areas of the pillar for hydrogen and nitrogen:

$$S_p = (A_{tot} - S)/N_p \quad (5)$$

These we compare with the pillar areas calculated by CHEM-X at different heights above the surface, to gauge the extent of adsorbed molecular penetration under the pillar.

(15) Nakahira, M. On the crystal structure of montmorillonite, with some references to other clay minerals. *J. Sci. Res. Inst. Tokyo* **1952**, *46*, 268–287 (from *Struct. Rep.* Wilson A. J. C., Ed.; **1952**, *16*, 367–368).

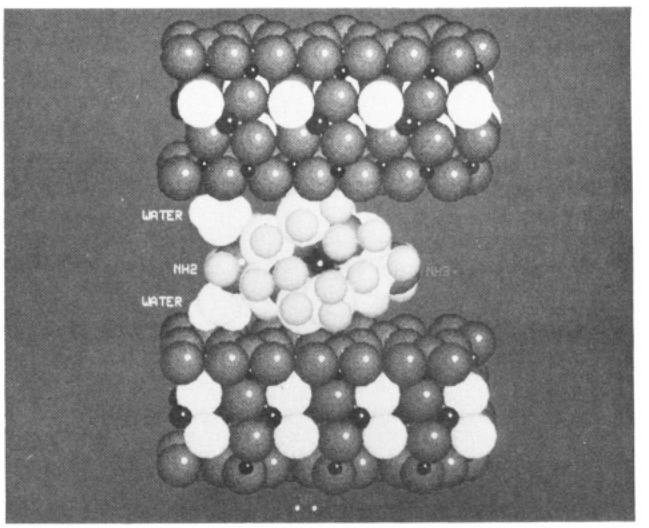

Figure 11. Model of (Hg-diamsarH)$^{3+}$ ion (on the left side NH_2 group and on the right side NH_3^+) between two clay layers in (Hg-diamsar)–fluorhectorite II. Interlayer distance corresponds to c spacing equal to 16.8 Å. Two water molecules shown on the level 2.3 Å from the surface (distance between surface oxygen and water hydrogen); hexagonal packing of the pillars; interpillar distance of 10.77 Å. The view is at an angle (about 6°) to the clay surface. The photograph is made from the terminal screen.

The calculated pillar cross sections and total effective areas occupied by the pillar at different heights above the surface are shown in Table III.

Nitrogen. When eq 5 is applied to the nitrogen data, pillar areas of ca. 170 ± 30 Å^2 are obtained for all systems except (Hg-diamsar)–montmorillonite I (S_p = 253 Å^2). As expected from Figure 8, top, the geometrical model with nitrogen packing on both clay surfaces and more or less space filling the interpillar region works well. Figure 10 shows that the nitrogen molecule does not penetrate under the "eaves" of the pillar, and Figure 7, looking at the pillar packing in plane, shows how the sieving effect develops with increased pillar density in the plane.

Water. The water molecules fits very well into the microporous structure created by dense pillar packing. The small value of S_p (43–50 Å^2) reflects this strong association.

Figure 11 shows a model of the (Hg-diamsar)$^{3+}$ ion and two molecules of water between two fluorhectorite layers. If we assume that the distance between clay surface oxygen and water should be equal to $D_{wat} = R_O + R_H$, where R_O and R_H are the radii of oxygen and hydrogen, respectively, D_{wat} = 2.3 Å. Estimation of the clay surface occupied by the Hg-diamsar pillar based on the structure of (Hg-diamsar)$^{4+}$ ion and calculated parallel to the clay plane at this contour level from the surface is 91.2 Å^2 for the chosen model A (Table III), while experimental S_p (about 50 Å^2) corresponds to a distance from the surface 1.5–1.7 Å and indicates a strong association of water with the pillar and the surface.

Hydrogen. The effective pillar areas calculated from the hydrogen BET surface areas are listed in Table IV. The low values of S_p for (Hg-diamsar)–fluorhectorite I and II compared to nitrogen can be explained by the accessibility of hydrogen beneath the pillars. This appears also to be true for (Co-sar)–fluorhectorite and may allow selective sieving of hydrogen and nitrogen.

Conclusions

For nitrogen and hydrogen adsorption the difference in size of adsorbates is of prime importance when the center–center interpillar distances in the fluorhectorites

change from 10.8 to 9.48 Å, so making the interpillar gas comparable with the size of adsorbing molecules. Thus in (Hg-diamsar)-montmorillonite I the interpillar distances are big enough (15 Å) that the size of the adsorbate does not influence the specific surface appreciably. The surface area measured by hydrogen adsorption is then almost equal to that measured by nitrogen. Adsorption of hydrogen may also be influenced by the charge on the pillar's amino groups. If clays have pillars with diprotonated amino groups, the S_{hyd}/S_{nit} ratio is much smaller. In general the S_{hyd}/S_{nit} ratio increases from 1.02 to 4.56 with a decrease in interpillar distances (d) from 15 Å in (Hg-diamsar)-montmorillonite I to 9.48 Å in (Hg-diamsar)-fluorhectorite III.

Acknowledgment. We thank C. Foudoulis for running X-ray powder diffraction, Dr. I. Creaser for her skill in making and for supplying us with the cage compounds, and Prof. T. Pinnavaia, Michigan State University, for the smaple of lithium-fluorhectorite sol.

Role of High-Resolution Electron Microscopy in the Identification and Characterization of New Crystalline, Microporous Materials: "Reading Off" the Structure and Symmetry Elements of Pentasil Molecular Sieves

Osamu Terasaki,*,† John M. Thomas,*,‡ G. Robert Millward,§ and D. Watanabe†

Department of Physics, Tohoku University, Aramaki-Aoba, Sendai 980, Japan, Davy Faraday Research Laboratory, The Royal Institution of Great Britain, 21 Albemarle Street, London W1X 4BS, England, and Department of Physical Chemistry, University of Cambridge, Lensfield Road, Cambridge CB2 1EP, England

Received September 13, 1988

The advantages of establishing the structure of new microporous, crystalline solids such as zeolites, porosils, and aluminum phosphates by using high-resolution electron microscopy are assessed and illustrated with reference to ZSM-5. In particular, it is shown that the structure and symmetry elements of this member of the pentasil family may, by comparison of computed and observed (at 200 and 1000 keV) images, be "read off" directly in real space. The technique is likely to be of especial value in characterizing many new structures, including those that, at the sub-unit-cell level, are composed of recurrent intergrowths of other structures.

The first synthesis of a zeolite with no natural counterpart was reported over 40 years ago.[1] In the intervening time more than 20 such zeolitic molecular sieves have been synthesized. In addition, apart from the naturally occurring and synthetic aluminosilicate molecular sieves, two other types of families of crystalline, microporous materials, called porosils and clathrasils,[2] have appeared on the scene. The porosils, through which molecules of small hydrocarbons may freely migrate, are the silica end-products of zeolites such as ZSM-5 and ZSM-11 (that is, silicalite I and silicalite II, respectively, the structures of which are shown in Figure 1). But they also encompass silica structures that may not have a zeolitic (aluminosilicate) counterpart. The clathrasils, on the other hand, typefied by naturally occurring melanophlogite and the recently synthesized nanosil and dodecasil 3C, possess intracrystalline cages the openings of which are too small to permit migration from cage to cage of the molecules that are trapped within these cavities as templates during synthesis.

Whereas the family of porosils continues to grow, its size is already dwarfed by yet another class of microcrystalline, microporous molecular sieves termed ALPOs, SAPOs, and MeALPOs—aluminum phosphates, silicon aluminum phosphates, and metal aluminum phosphates, respectively—first reported by workers at the Union Carbide Laboratories.[3,4] These consist of three-dimensional, four-connected (corner-sharing) tetrahedra of AlO_4 and PO_4 in the case of the ALPOs. The structures of some members of this large family are the same as their zeolitic (aluminosilicate and synthesized gallosilicate or aluminogermanate) counterparts, but others within the family are quite novel. Some 20 or so elements of the periodic table, including Li, Be, Ga, Si, As, Zn, Co, and Mg, can be accommodated in the framework of these porous aluminum phosphates, yielding a broad range of molecular sieves.

The majority of all these microporous solids can seldom be induced to grow as single crystals suitable for X-ray structural analysis, so that alternative, somewhat unconventional and certainly multipronged methods of structural analysis have to be utilized. These methods[5-7] entail the use of powder (X-ray and neutron) diffraction, solid-state NMR, and a range of other spectroscopies as well as high-resolution electron microscopy. Once a plausible

† Tohoku University.
‡ The Royal Institution of Great Britain.
§ University of Cambridge.

(1) Barrer, R. M. British Patent 574, 1946.
(2) Liebau, F. *Structural Chemistry of Silicates*; Springer: Berlin, 1985.
(3) Wilson, S. T.; Lok, B. M.; Messina, C. A.; Cannan, T. R.; Flanigan, E. M. Intrazeolite Chemistry. *ACS Symp. Ser.* **1983**, *218*, 79.
(4) Flanigan, E. M.; Lok, B. M.; Patton, R. L.; Wilson, S. T. In *New Developments in Zeolite Science and Technology*; Murakami, Y., Iijima, A., Ward, J. W., Eds.; Elsevier: Amsterdam, 1986; p 103.
(5) Thomas, J. M. *Proc. 8th Int. Conf. Catal., Berlin* **1984**, *1*, 31.
(6) Thomas, J. M.; Klinowski, J. *Adv. Catal.* **1985**, *33*, 197.
(7) Thomas, J. M.; Catlow, C. R. A. *Prog. Inorg. Chem.* **1987**, *35*, 1.

0897-4756/89/2801-0158$01.50/0